Arabian Journal of Chemistry (2021) **14**, 103224

King Saud University

Arabian Journal of Chemistry

www.ksu.edu.sa
www.sciencedirect.com

ORIGINAL ARTICLE

Cu immobilized on chitosan-modified iron oxide magnetic nanoparticles: Preparation, characterization and investigation of its anti-lung cancer effects

Zonghua Shi [a], Yousef Mahdavian [b,*], Yasamin Mahdavian [c], Siavash Mahdigholizad [d], Parisa Irani [e], Mohammad Karimian [f], Naser Abbasi [g], Hori Ghaneialvar [g,h], Akram Zangeneh [g], Mohammad Mahdi Zangeneh [g]

[a] *Department of Critical Care Medicine, The Fifth Affiliated Hospital of Zhengzhou University, Zhengzhou, Henan Province 450052, China*
[b] *Department of Chemistry and Physics, Mount Royal University, Calgary, Alberta, Canada*
[c] *Department of Applied Chemistry, Faculty of Pharmaceutical Chemistry, Tehran Medical Sciences, Islamic Azad University, Tehran, Iran*
[d] *School of Medicine, Iran University of Medical Sciences, Tehran, Iran*
[e] *Department of Chemistry, Payame Noor University, Tehran, Iran*
[f] *Department of General Surgery, Faculty of Medicine, Ilam University of Medical Sciences, Ilam, Iran*
[g] *Biotechnology and Medicinal Plants Research Center, Ilam University of Medical Sciences, Ilam, Iran*
[h] *Department of Clinical Biochemistry, Faculty of Medicine, Ilam University of Medical Sciences, Ilam, Iran*

Received 8 December 2020; accepted 17 May 2021
Available online 2 June 2021

KEYWORDS

Copper;
Chitosan;
Magnetic nanocomposite;
Antioxidant assay;
Lung cancer

Abstract Chitosan is a linear polysaccharide and non-toxic bioactive polymer with a wide variety of applications due to its functional properties such as ease of modification, and biodegradability. In this study, a green protocol for supporting of Cu(II) on chitosan-encapsulated magnetic Fe_3O_4 nanoparticles is described. The morphological and physicochemical features of the material were determined using several advanced techniques like fourier transformed infrared spectroscopy (FT-IR), field emission scanning electron microscopy (FESEM), transmission electron microscopy (TEM), energy dispersive X-ray spectroscopy (EDS), X-ray diffraction (XRD), inductively coupled plasma (ICP), vibrating sample magnetometer (VSM) and X-ray photoelectron spectroscopy

* Corresponding author.
E-mail address: yousof.mhdvn@gmail.com (Y. Mahdavian).
Peer review under responsibility of King Saud University.

Production and hosting by Elsevier

https://doi.org/10.1016/j.arabjc.2021.103224
1878-5352 © 2021 Published by Elsevier B.V. on behalf of King Saud University.
This is an open access article under the CC BY-NC-ND license (http://creativecommons.org/licenses/by-nc-nd/4.0/).

(XPS). The average diameter of the NPs was approximately 15–25 nm. In addition, the Fe_3O_4/CS/Cu (II) nanocomposite was engaged in biological assays like study of anti-oxidant properties by DPPH mediated free radical scavenging test using BHT as a reference molecule. Thereafter, on having a significant IC_{50} value in radical scavenging assay, we extended the bio-application of the desired nanocomposite in anticancer study of lung well-differentiated bronchogenic adenocarcinoma, lung moderately differentiated adenocarcinoma, and lung poorly differentiated adenocarcinoma of human lung *in-vitro* conditions. In the cytotoxicity and anti-human lung studies, the nanocomposite was treated to lung cancer lung well-differentiated bronchogenic adenocarcinoma (HLC-1), lung moderately differentiated adenocarcinoma (LC-2/ad), and lung poorly differentiated adenocarcinoma (PC-14) cell line following MTT assay. The cell viability of malignant lung cell line reduced dose-dependently in the presence of Fe_3O_4/CS/Cu(II) nanocomposite. The recent results suggest that Fe_3O_4/CS/Cu(II) nanocomposite have a suitable anticancer activity against lung cell lines.

© 2021 Published by Elsevier B.V. on behalf of King Saud University. This is an open access article under the CC BY-NC-ND license (http://creativecommons.org/licenses/by-nc-nd/4.0/).

1. Introduction

In human respiratory system lung is an imperative organ that is actively involved in the crucial transfusion of O_2 and CO_2 into blood (World Cancer Research Fund and American Institute for Cancer Research, 2007; Thun et al., 2018). Improper functioning of lungs majorly occurs due to flu, asthma, bronchitis, pneumonia, tuberous sclerosis, cystic fibrosis, chronic obstructive pulmonary disease (COPD), tuberculosis, emphysema and cancer. Lung cancer is one of the most invasive and metastasizing cancer and one of the major reason of mortality in the world. It is the third most common cancers after breast and prostate in terms of fatality and affects both men and women (Alaoui et al., 2015). The common symptoms for lung cancer are weakness, loss of weight, fatigue, coughing up blood, hoarseness, wheezing, chest pain and dysphagia (Hecht, 2012; Alsharairi, 2019). Chemotherapy, radio therapy, targeted therapy, immunotherapy and surgery are the general therapeutic treatments for lung cancer patients (Jones and Baldwin, 2018). Nevertheless, due to severe side effects of the treatment procedures like damage of nerves, toxicity, hair loss, fatigue, diarrhea and mouth sore, it has been a serious concern among the researchers to find out new formulations (Stahl, 2013). While searching for unconventional remedies, it has been found that metal nanoparticles (MNP), being tender to our biological systems, display brilliant anticancer properties (Abdel-Fattah and Ali, 2018; Patil and Kim, 2017; Bisht and Rayamajhi, 2016; Hassanien et al., 2018). From then on, a high end-research has been conceded worldwide to develop MNPs and nanocomposites for the treatment of different cancers including human CRC.

In addition to the wide applicability of nanomaterials in catalysis and environmental issues, in recent times they also have been observed to exhibit interesting biomedical applications in tissue engineering, photoablation therapy, bioimaging, hyperthermia, medicinal therapeutics (McNamara and Tofail, 2016; McNamara et al., 2013; McNamara and Tofail, 2015). Due to nano-dimensions, NPs can easily surpass the cell barrier and also due to high surface area they are used as excellent carriers of different hydrophobic and hydrophilic drugs, biomolecules like vaccines, hormones etc to different administrations (Issa et al., 2013; Baygar and Ugur, 2017; Shanmugasundaram et al., 2013; Zou et al., 2015; Karamipour et al., 2015; Jia et al., 2012; Tansık et al., 2014). The NPs facilitate this delivery process by stimulating the drug and also stabilizing them to reach the target cell (Surendra et al., 2014; Sabale et al., 2015). Some NPs function as sensors in diagnosis of ailments, detection of DNA and antibodies (Park et al., 2014; Govindaraju et al., 2015; Patra et al., 2015; Aygün et al., 2020). Recently, surface engineered functionalized NPs have been found to show remarkable anticancer activities, in particular, the cancer of lung, prostate, ovarian and leukemia (Manjunath and Joshi, 2019; Sriramulu and Sumathi, 2017; Netala et al., 2016). Surface designing of NPs using different biomolecules and organic ligands have been an excellent idea in order to improve the binding the drugs and other molecules and also to target the antibodies in the effective treatment of cancers.

Chitosan is a naturally occurring polymer with several electron rich polar functional groups like amino (NH_2) and hydroxyl (OH) that used very well for synthesis and stabilizing of various metal nanoparticles (Karthikeyan et al., 2020; Khan et al., 2020). These very features of the functionalized NPs have encouraged us to design and demonstrate a novel Cu (II) immobilized chitosan (CS) modified-magnetite nanoparticles (Fe_3O_4/CS/Cu(II)). The biopolymer (CS) was exploited to create a shell over the pre-synthesized Fe_3O_4 NPs. Glutaraldehyde to use in this protocol to build a compact imino bridged structure between the successive layers of CS. The super polar environment (OH, NH_2 groups) as created was subsequently used to bind the incoming Cu (II) ions affording the nanocomposite. Now, towards the bio-applications, we employed the as-architectured material to study the cytotoxicity against lung cancer cell line though an MTT assay. Interestingly, we acquired outstanding potential of the material as an unconventional formulation towards the treatment of lung cancer.

2. Experimental

2.1. Materials and apparatus

All the reagents were purchased from Aldrich and Merck and were used without any purification. CS, copper nitrate, sodium hydroxide and all the other chemicals were purchased from Sigma-Aldrich. In instrumental section, the particle size, morphology and atomic mapping analysis of the nanomaterial was investigated using a FESEM-TESCAN MIRA3 microscope equipped with EDX. The crystalline structures of the samples

were evaluated by X-ray diffraction (XRD) analysis on a Bruker D8 Advance diffractometer with CuKα radiation at 40 kV and 20 mA. Fourier transform infrared (FT-IR) spectra were recorded with a Perkin Elmer 65 spectrometer in the range of 400–4000 cm^{-1}. Transmission electron microscopy (TEM) analysis was performed on a Phillips CM10 microscope at an accelerating voltage of 200 kV. Magnetization measurements were carried out on a BHV-55 vibrating sample magnetometer (VSM).

2.2. Preparation of Fe_3O_4 NPs

Its prepared according the literature Karthikeyan et al. (2020) with some modification. Magnetite nanoparticles (Fe_3O_4) were prepared by stirring $FeSO_4$š$7H_2O$ (2.1 g) and $FeCl_3$š$6H_2O$ (3 g) in water (100 mL) at 80 °C for 30 min. Then, 5 mL of anhydrous ammonia was added into the reaction medium and the mixture was stirred at 80 °C for 30 min. Afterwards, Fe_3O_4 was separated, washed with water to neutrality and dried at 50 °C for 12 h.

2.3. Preparation of Fe_3O_4/CS/Cu(II) nanocomposite

0.5 g Fe_3O_4 NP were dispersed in 50 mL deionized water. A 30 mL homogeneous mixture of chitosan (98% deacetylated, 4.3542×10^4 g/mol) in acetic acid solution (0.2 g CS in 50 mL 1% HOAc) was added to the dispersion. The resulted solution was stirred vigorously and subsequently a glutaraldehyde aqueous solution (5 wt%, 10 mL) was added drop by drop and stirred for 60 min at 50 °C. The solid sample was collected by external magnet, washed with ethanol for several times to remove residual impurities and then left to dry at 60 °C for 24 h affording a brown-colored solid. In the final step, 0.5 gm of Fe_3O_4/CS composite was dispersed in 100 mL H_2O by ultrasonication for 20 min. Subsequently, an aqueous solution of $Cu(NO_3)_2$ (1 mmol in 20 mL H_2O) was added to reaction mixture and stirred for 5 h at 25 °C. Then, the mixture was cooled and the final material Fe_3O_4/CS/Cu (II) nanocomposite were collected using a magnet. Subsequently, they were washed with distilled water and dried at ambient temperature. The Cu load was 0.23 mmol/g as was determined by ICP-OES.

2.4. Determination of antioxidant property of Fe_3O_4/CS/Cu(II) nanocomposite

The DPPH method is a common method for the assessment of the antioxidant activity of plant species and metallic nanoparticles. It is based on trapping the free radicals of the material, called DPPH, using antioxidant agents which reduce the absorption rate at 520 nm wavelength. When the DPPH solution is mixed with a material that can donate hydrogen atom, radical resuscitation is formed, which is followed by color reduction. This reaction eliminates the purple color; whose index is the formation of an absorption band at 520 nm (Mahdavi et al., 2019).

To determine the radical scavenging activity of the Fe_3O_4/CS/Cu(II) nanocomposite, 1 mL of 50 μm DPPH was combined with 1 mL of variable concentrations (0–1000 μg/mL) of Fe_3O_4/CS/Cu(II) nanocomposite. Then, they were transferred to the 37 °C for 1 h. The samples absorption rate was determined at 520 nm by a spectrophotometer, and the antioxidant activity was calculated by the below formula:

$$\text{Inhibition}(\%) = \frac{\text{SampleA.}}{\text{ControlA.}} x100$$

The blank sample contained 1 mL methanol and 1 mL Fe_3O_4/CS/Cu(II) nanocomposite, and a sample of 1 mL DPPH and 2 mL of Fe_3O_4/CS/Cu(II) nanocomposite with the applied concentrations was regarded as the negative control (Mahdavi et al., 2019).

Calculation of half-maximal inhibitory concentration (IC50) is a suitable method for comparison of the activity of pharmaceutical materials. In this method, the measurement and comparison criterion is the concentration in which 50% of the final activity of the drug occurs. In this experiment, the IC50 of various repeats is estimated and compared with the IC50 of BHT, which is introduced as the antioxidant activity index. The closer is the obtained value to the IC50 of BHT, the stronger is the antioxidant activity of the material. The graph of the IC50 of the extract was produced by drawing the percent inhibition curve versus the extract concentration. First, three stock samples with variable concentrations (0–10 00 μg/mL) of Fe_3O_4/CS/Cu(II) nanocomposite were prepared. Then, a serial dilution was prepared from each sample, and IC50 of the above samples was measured separately, following which their mean was calculated. BHT, with different concentrations, was considered positive control. All experiments were performed in triplicate (Mahdavi et al., 2019).

2.5. Determination of anti-human lung cancer effects of Fe_3O_4/CS/Cu(II) nanocomposite

The human lung cancer cell lines (Lung well-differentiated bronchogenic adenocarcinoma: HLC-1, Lung moderately differentiated adenocarcinoma: LC-2/ad, and Lung poorly differentiated adenocarcinoma: PC-14) and the normal cell line (HUVEC) in the MTT assay were used as follows. They were then cultured as a monolayer culture in 90% RPMI-1640 medium and 10% fetal serum and supplemented with 200 mg/mL streptomycin, 125 mg/mL penicillin, and 8 mg/mL amphotericin B. The culture was then exposed to 0.5 atmospheric carbon dioxide at 37 °C, on which the tests were performed after at least ten successful passages. MTT assay a method used to investigate the toxic effects of various materials on various cell lines, including non-cancer and cancer cells. To evaluate the cell toxicity effects of the compounds used in this research, the cells were transferred from the T25 flask to the 96-well flasks. In each cell of the 96-cell flasks, 7000 cells of cancer and fibroblast cell lines were cultured, and the volume of each cell was eventually increased to 100 μL. Before the treatment of the cells in the 96-well flak, the density of cells was increased to 70%, so the 96-well flasks were incubated for 24 h to obtain the cell density of 7×10^3. Next, the initial culture medium was discarded, and variable concentrations (0–1000 μg/mL) of Fe_3O_4/CS/Cu(II) nanocomposite were incubated at 37 °C and 0.5 CO_2 for 24, 48, and 72 h. Then, 20 μL MTT was added

to each well after a certain amount of time. Next, 100 µL DMSO solvent was added to each well. They were then kept at room temperature for 25 min and read at 490 and 630 nm by a microtitre plate reader (Mahdavi et al., 2019).

The cell lines were treated with the hydroalcoholic extract (1.25 mg/mL), which inhibited about 20% of the cell growth. Annexin/PI method was used to determine the apoptosis level in the treated and control cell lines using a flow cytometry machine. To perform experiment, the cell lines were treated with a variable concentrations (0–1000 µg/mL) of Fe_3O_4/CS/Cu(II) nanocomposite for 24 h. Cells were irrigated with phosphate-buffered saline (PBS). After centrifugation, buffer binding was added to the obtained precipitate. Then, 5 µL Annexin V dye was added and incubated for 15 min at 25 °C. Cells were washed with the binding solution, following which 10 µL PI dye was added. Finally, cell analysis was done by a flow cytometry machine according to the below formula:

$$\text{Cellviability}(\%) = \frac{\text{SampleA.}}{\textit{ControlA.}} x100$$

3. Results and discussion

3.1. Analysis of catalytic characterization data

After the post-grafting synthesis of Fe_3O_4/CS/Cu(II) nanocomposite (Fig. 1), the physicochemical characteristics and structural morphology were thoroughly studied using various analytical techniques like FT-IR, FE-SEM, EDX, elemental mapping, TEM, VSM, XPS, XRD and ICP-AES. Fig. 2 represents the FT-IR spectrum of the final nanocomposite and its two precursor components in a single frame in order to justify the structure. Fig. 2a shows the characteristic peaks of Fe_3O_4 at 584 and 632 cm^{-1} attributed to Fe-O stretching vibration of spinel structure. The representative peaks of chitosan is shown in Fig. 2b, being appeared at 1033 cm^{-1}, 1385 cm^{-1}, 1616 cm^{-1}, 1739 cm^{-1} and 3400–3500 cm^{-1}, corresponding to C–N, C–O stretching, N-H bending, C = O and O-H stretching vibrations respectively. In the spectrum of Fe_3O_4/CS/Cu(II), the previous two components have been evi-

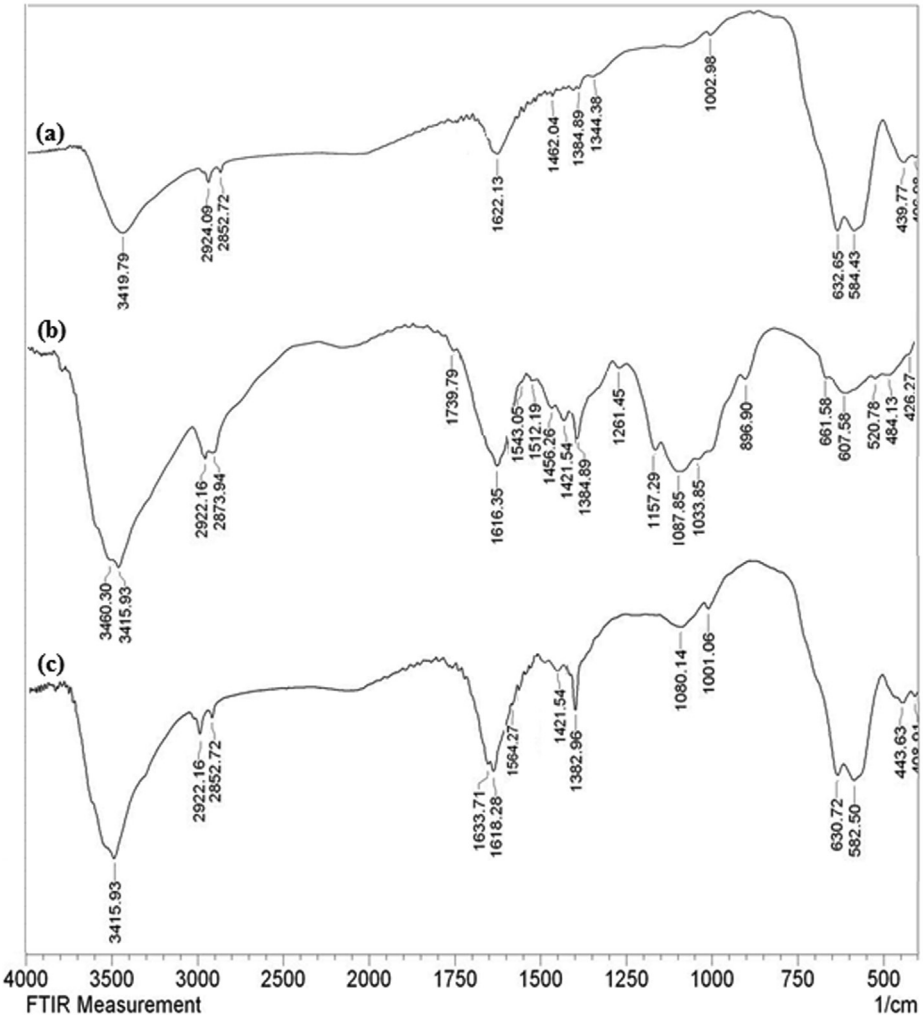

Fig. 1 Schematic fabrication of magnetic Fe_3O/CS/Cu(II) nanocomposite.

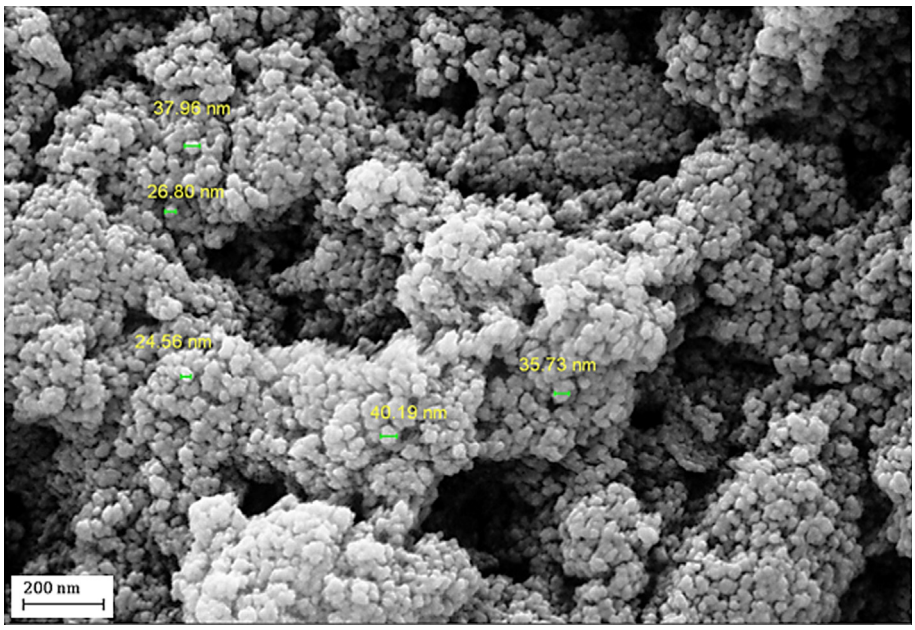

Fig. 2 FT-IR spectra of a) Fe_3O_4, b) CS and c) Fe_3O_4/CS/Cu(II) nanocomposite.

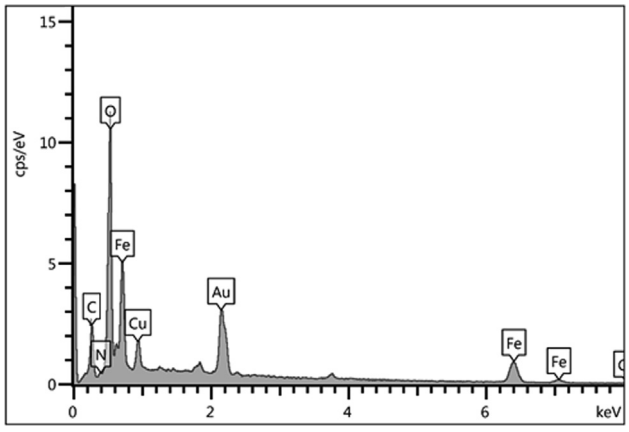

Fig. 3 FESEM image of Fe_3O_4/CS/Cu(II) nanocomposite.

dently intermingled with slight shifting of vibrations. It validates the unified and stable structure being formed with those parts. The imino bonds (C = NH) formed during intermolecular cross-linking can be observed at 1633 cm^{-1}. The deviation in vibrations in the final material is anticipated due to strong chelation with Cu NPs with the organofunctions.

FE-SEM analysis of Fe_3O_4/CS/Cu (II) NPs was carried out to resolve its surface morphology, texture and particle size (Fig. 3). It displays the quasi-spherical nano-dimensional particle units of mean particle size 25–35 nm. From close vicinity, a thin continuous layer of CS over the core Fe_3O_4 can be identified. The aggregation of particles can be adjudged due to manual sample preparation. An EDX instrument equipped with the FESEM was used to ascertain the elemental composition of Fe_3O_4/CS/Cu (II) NPs (Fig. 4). The EDX profile clearly shows the presence of Fe, Cu, C, N and O as the constituting elements. As the sample is Au coated during analysis, it appears in the profile by default. C, N and O validates the successful surface functionalization with CS. Now, the results of EDX analysis was further confirmed by elemental mapping study. A sectional scanning of SEM image reveals the distribution of the comprising elements, being represented in Fig. 5. The colored dots signify the corresponding atoms which are uniformly spread over the whole surface.

The intrinsic structural features of the Fe_3O_4/CS/Cu(II) nanocomposite are demonstrated though TEM analysis (Fig. 6). The particles are roughly globular and within the size range of 15–20 nm, being compatible with the FESEM results. However, the surface functionalization could not be detected from the image.

Magnetic properties of the Fe_3O_4/CS/Cu(II) nanocomposite were appraised by VSM analysis. When a variable magnetic field (−20 kOe to +20 kOe) was applied on the material at 300 K, a hysteresis curves was obtained, being shown in Fig. 7. It clearly denotes the superparamagnetic nature of the material having magnetization saturation (M_s) value of 32.6. Due to surface coating by the non-magnetic CS, M_s value is observed low as compared to standard unmodified ferrite NPs.

Electronic environment, binding energy and oxidation states of the active species in the material was ascertained by XPS technique (Fig. 8). The 2p region of Cu splits up into two spin-orbit components, namely, $2p_{3/2}$ and $2p_{1/2}$ and the corresponding binding energies obtained from the nanocomposite was compared with the standard peak positions. The two sharp peaks are observed at 933.61 eV and 943.12 eV respectively indicating that Cu is in the formal +2 valance state (Baygar and Ugur, 2017).

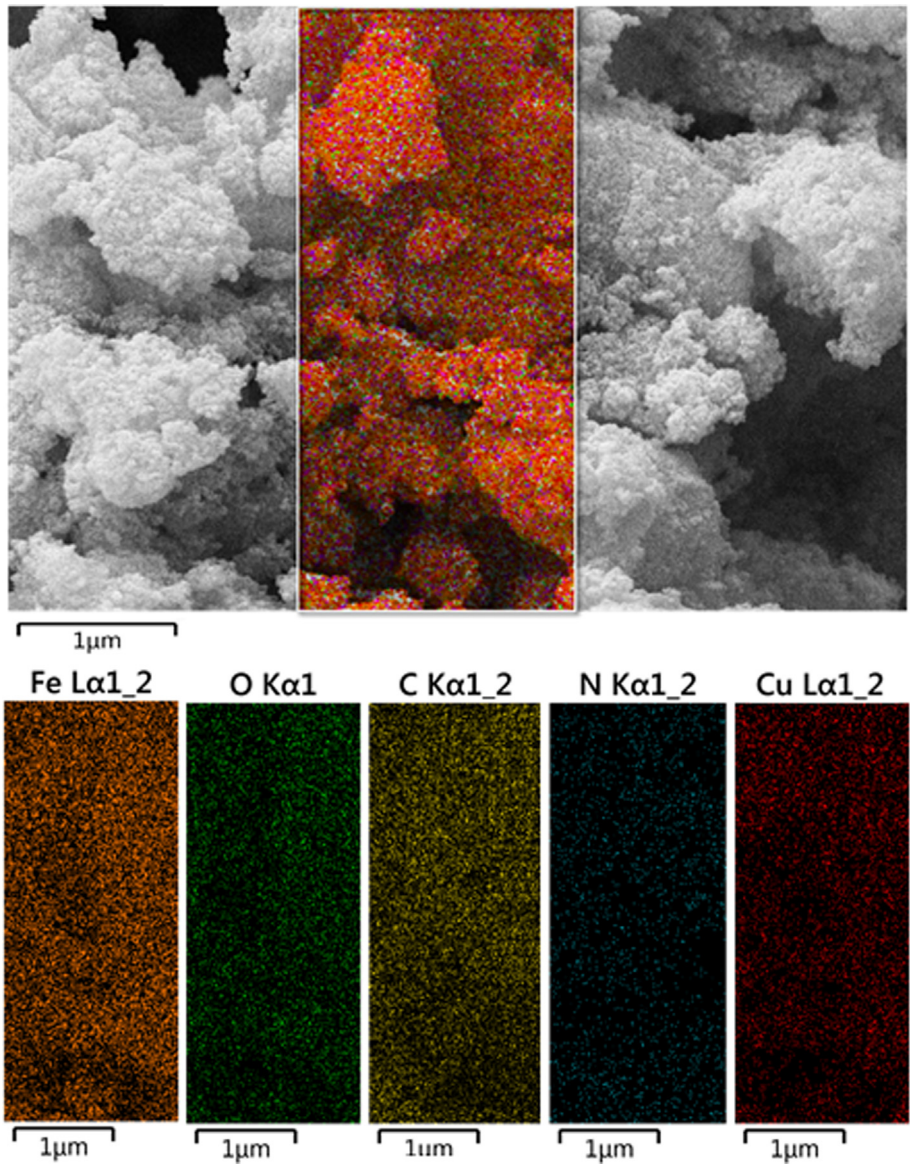

Fig. 4 EDX pattern of Fe_3O_4/CS/Cu(II) nanocomposite.

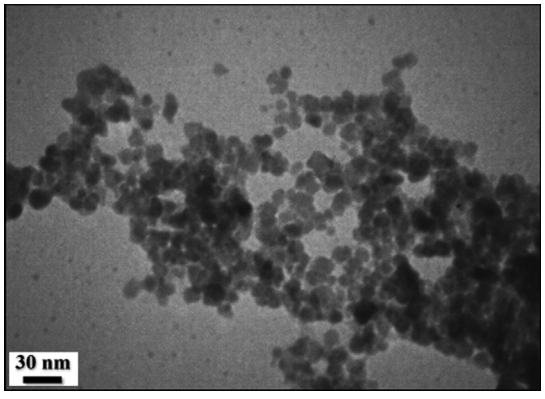

Fig. 5 Elemental mapping of Fe_3O_4/CS/Cu(II) nanocomposite, Fe, O, C, N and Cu respectively.

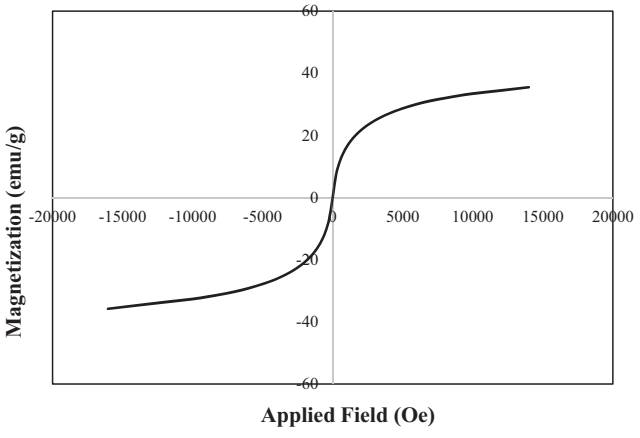

Fig. 6 TEM images of Fe_3O_4/CS/Cu(II) nanocomposite.

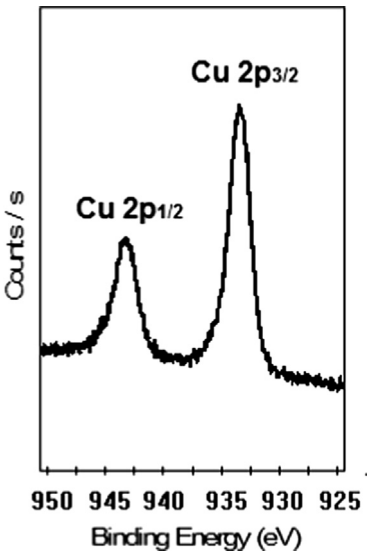

Fig. 7 VSM analysis of Fe_3O_4/CS/Cu(II) nanocomposite.

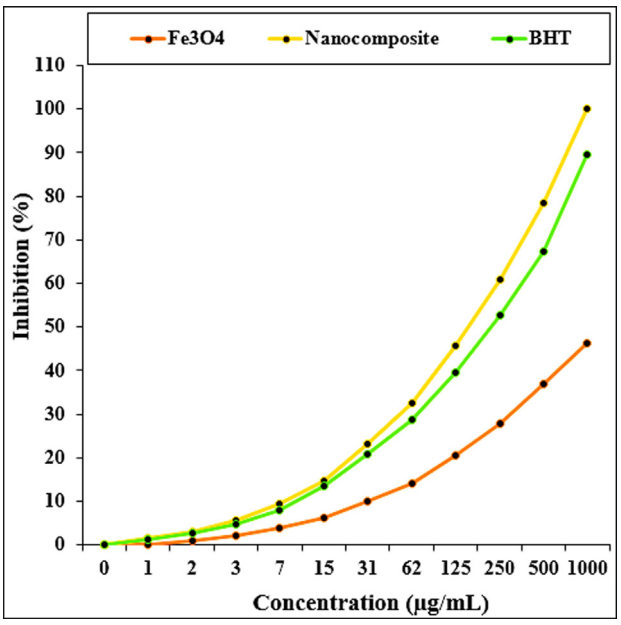

Fig. 9 XRD patterns of (a) Fe_3O_4 and (b) Fe_3O_4/CS/Cu(II) nanocomposite.

Finally, the crystallinity and phase structure of the Fe_3O_4/CS/Cu(II) nanocomposite were determined by XRD analysis. In Fig. 9, the diffraction peaks of bare Fe_3O_4 was compared to the final material. As can be seen from Fig. 9a, the characteristic peaks of Fe_3O_4 NPs appears at $2\theta = 30.6°$, 36.2°, 43.7°, 54.1°, 57.4° and 63.5° due to diffraction on the (220), (311), (400), (422), (511) and (440) planes (JCPDS No. 19-0629). In the XRD profile of Fe_3O_4/CS/Cu(II), all the very peaks of Fe_3O_4 NPs are present indicating the un-deformed core structure even after post-modifications. The initial broad region till 20° are contributed from CS. Additionally, the weak diffraction peaks at $2\theta = 43.2°$, 50.5° and 74.4° correspond to the (111), (200) and (220) planes of crystalline Cu phases (JCPDS No.04–0784).

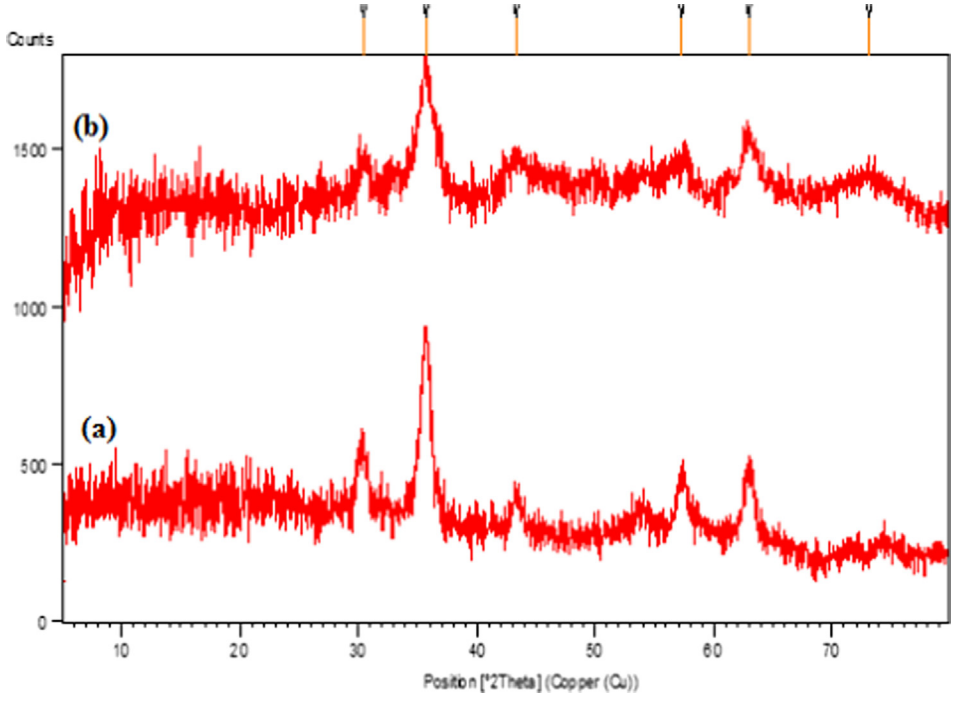

Fig. 8 XPS scan in the Cu 2p region for Fe_3O_4/CS/Cu(II) nanocomposite.

3.2. Antioxidant, cytotoxicity and anti-human lung cancer potentials of Fe_3O_4/CS/Cu(II) nanocomposite

In this study, the concentration-dependent DPPH radical scavenging effect of Fe_3O_4/CS/Cu(II) nanocomposite was analyzed with respect to a standard molecule (BHT). The interaction between Fe_3O_4/CS/Cu(II) nanocomposite and DPPH might have occurred by transferring electrons and hydrogen ions (Mahdavi et al., 2019). The scavenging capacity of the Fe_3O_4/CS/Cu(II) nanocomposite and BHT at different concentrations, expressed in terms of percentage inhibition, has been plotted in Table 1 and Fig. 10. The corresponding IC_{50} values of BHT and Fe_3O_4/CS/Cu(II) nanocomposite were found 230 and 162 μg/mL, respectively.

In the recent research, the treated cells with several concentrations of the present of Fe_3O_4 and Fe_3O_4/CS/Cu(II) nanocomposite were examined by MTT test for 72 h regarding the cytotoxicity properties on HLC-1, LC-2/ad, and PC-14. The absorbance rate was determined at 545 nm, which indicated extraordinary viability on HLC-1, LC-2/ad, and PC-14 cell line even up to 1000 μg/mL nanocomposites (Table 2, Fig. 11, Scheme 1). The results showed, the viability of them reduced dose-dependently in the presence of Fe_3O_4/CS/Cu(II) nanocomposite. The IC50 of Fe_3O_4/CS/Cu(II) nanocomposite were 252, 233, and 128 μg/mL against HLC-1, LC-2/ad, and PC-14 cell line, respectively (Table 2, Fig. 11, Scheme 1).

Table 1 The IC50 of Fe_3O_4, nanocomposite, and BHT in antioxidant test.

	Fe_3O_4 (μg/mL)	Nanocomposite (μg/mL)	BHT (μg/mL)
IC50 against DPPH	–	162	230

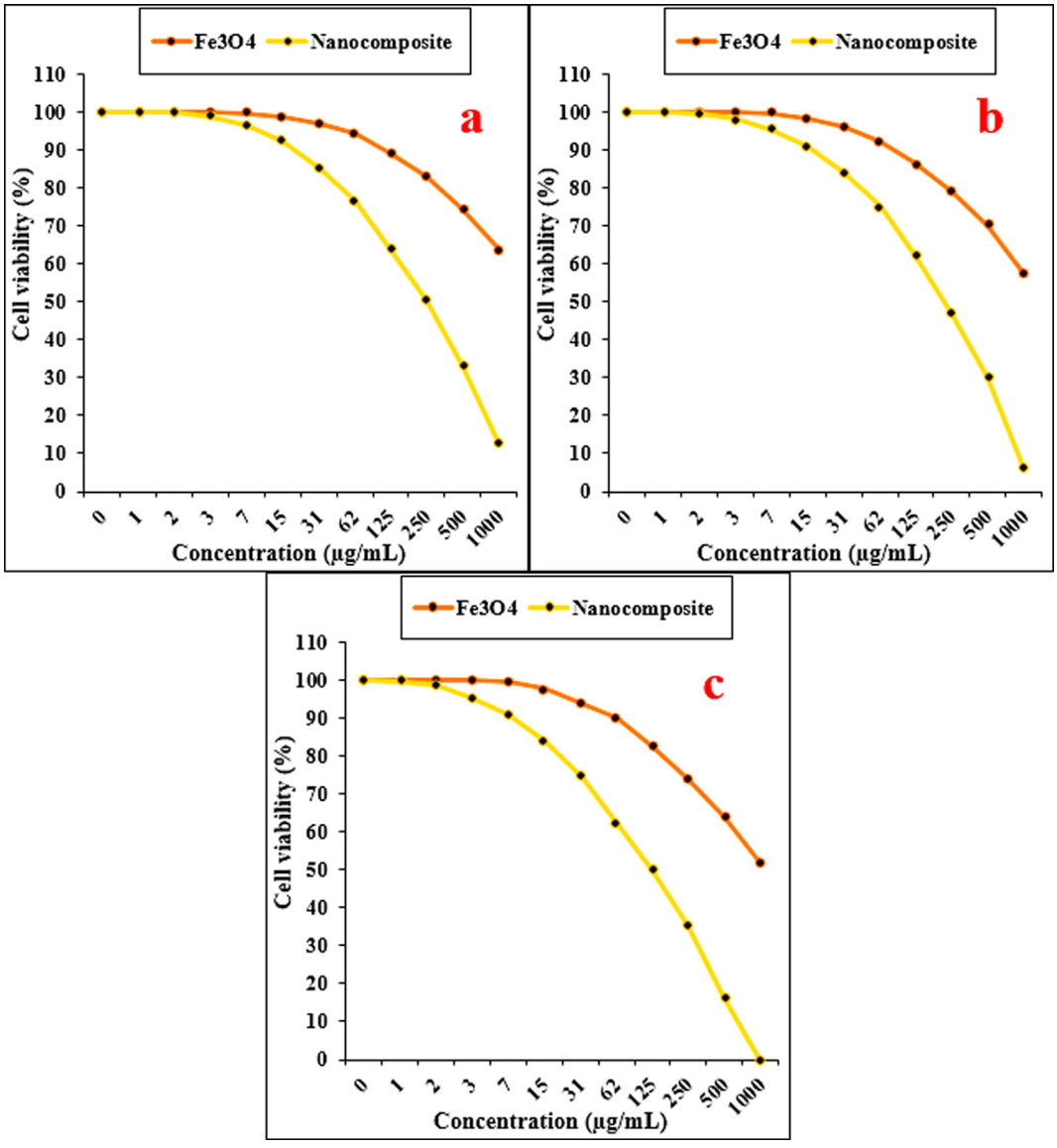

Fig. 10 The antioxidant properties of Fe_3O_4, nanocomposite, and BHT against DPPH.

Table 2 The IC50 of Fe_3O_4 and nanocomposite in the anti-human lung adenocarcinoma test.

	Fe_3O_4 (μg/mL)	Nanocomposite (μg/mL)
IC50 against MCF7	–	252
IC50 against Hs 578Bst	–	233
IC50 against Hs 319.T	–	128
IC50 against HUVEC	813	–

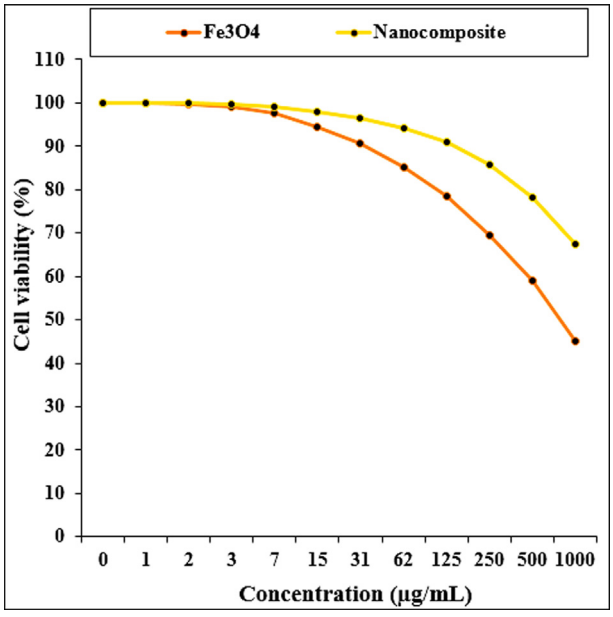

Fig. 11 The anti-human lung adenocarcinoma properties of Fe_3O_4 and nanocomposite against HLC-1 (a), LC-2/ad (b), and PC-14 (c) cell lines.

The anticancer potentials of Fe_3O_4/CS/Cu(II) nanocomposite against human lung cancer cell lines are linked to their antioxidant properties. Several different studies have revealed the strong antioxidant materials such as Cu and Fe nanoparticles significantly reduces the volume of tumors by removing free radicals (Mahdavi et al., 2019; Beheshtkhoo et al., 2018; Sangami and Manu, 2017). Our successful effort in exploiting Fe_3O_4/CS/Cu(II) nanocomposite in lung cancer studies will definitely enlighten the future studies in this arena.

4. Conclusions

In summary, we demonstrate the synthesis of Fe_3O_4/CS/Cu (II) nanocomposite by post-synthetic coordinating Cu(II) ions over chitosan modified magnetic nanoparticles. The material was characterized using several advanced physico-chemical methods. FESEM and TEM analysis justified the grafting of CS over the core ferrite NPs. The incoming Cu species was in ionic +2 state, as confirmed from XPS analysis. XRD analysis validated the united crystalline nanocomposite with all its possible characteristic diffraction peaks. The nanocomposite was also explored biologically in the antioxidant and anticancer assays. In the cytotoxicity and anti-human lung studies, the nanocomposite was treated to lung cancer cell lines following MTT assay. The cell viability of malignant lung cell line reduced dose-dependently in the presence of Fe_3O_4/CS/Cu(II) nanocomposite. IC50 values of the nanocomposite were observed to be 915.22 μg/mL against lung well-differentiated bronchogenic adenocarcinoma (HLC-1), lung moderately differentiated adenocarcinoma (LC-2/ad), and lung poorly differentiated adenocarcinoma (PC-14) cell lines. The outstanding results showed by the developed nanocomposite, could be highly promising in cancer management in near future.

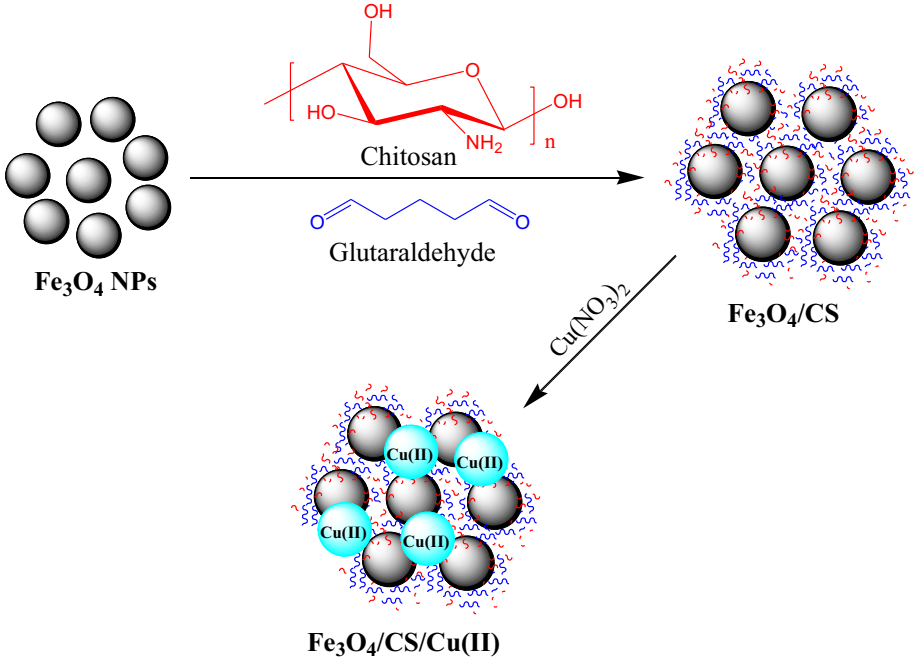

Scheme 1 The cytotoxicity effects of Fe_3O_4 and nanocomposite against normal (HUVEC) cell line.

Declaration of Competing Interest

The authors declare that they have no known competing financial interests or personal relationships that could have appeared to influence the work reported in this paper.

References

Abdel-Fattah, W.I., Ali, G.W., 2018. J. Appl. Biotechnol. Bioeng. 5 (2), 00116.

Alaoui, H.L., Hassan, O., Yang, Y.-W., Buchanan, P., 2015. Biochim. Biophys. Acta 1856 (2), 189–210.

Alsharairi, N.A., 2019. Nutrients 11, 725.

Aygün, A., Özdemir, S., Gülcan, M., Cellat, K., Sen, F., 2020. J. Pharm. Bimed. Anal. 178, 112970.

Baygar, T., Ugur, A., 2017. IET Nanobiotechnol. 11, 286–291.

Beheshtkhoo, N., Kouhbanani, M.A.J., Savardashtaki, A., et al, 2018. Appl. Phys. A 124, 363–369.

Bisht, G., Rayamajhi, S., 2016. Nanobiomedicine 3, 1–11.

Govindaraju, K., Krishnamoorthy, K., Alsagaby, S.A., Singaravelu, G., Premanathan, M., 2015. IET Nanobiotechnol. 2015, 1.

Hassanien, R., Husein, D.Z., Al-Hakkani, M.F., 2018. Heliyon 12, e01077.

Hecht, S.S., 2012. Int. J. Cancer 131, 2724–2732.

Issa, B., Obaidat, I.M., Albiss, B.A., Haik, Y., 2013. Int. J. Mol. Sci. 14, 21266.

Jia, Y., Yuan, M., Yuan, H., Huang, X., Sui, X., Cui, X., Tang, F., Peng, J., Chen, J., Lu, S., Xu, W., Zhang, L., Guo, Q., 2012. Int. J. Nanomedicine 7, 1697.

Jones, G.S., Baldwin, D.R., 2018. Clin. Med. 18, 41–46.

Karamipour, S., Sadjadi, M.S., Farhadyar, N., 2015. Spectrochim. Acta Mol. Biomol Spectrosc. 148, 146.

Karthikeyan, C., Varaprasad, K., Akbari-Fakhrabadi, A., Haja Hameed, A.S., Sadiku, R., 2020. Carbohydr. Poly. 249, 116825; (b) Jayaramudu, T., Varaprasad, K., Pyarasani, R.D., Reddy, K. K., Kumar, K.D., Akbari-Fakhrabadi, A., Mangalaraja, R.V., Amalraj, J., 2019. Int. J. Biol. Macromol. 128, 499–508; (c) Baran, T., Nasrollahzadeh, M., 2019. Carbohydr. Poly. 222, 115029.

(a) Khan, M.S.J., Khan, S.B., Kamal, T., Asiri, A.M, 2020. J. Poly. Environ. 28, 962–972; (b) Khan, M.S.J., Kamal, T., Ali, F., Asiri, A.M., Khan, S.B., 2019. Int. J. Biol. Macromol. 132, 772-783; (c) Ali, F., Khan, S.B., Kamal, T., Alamry, K.A., Bakhsh, E.M., Asiri, A.M., Sobahi, T.R.A., 2018. Carbohydr. Poly. 192, 217–230; (d) Khan, S.B., Ali, F., Kamal, T., Anwar, Y., Asiri, A.M., Seo, J., 2016. Int. J. Biol. Macromol. 88, 113–119; (e) Kamal, T., Anwar, Y., Khan, S.B., Chani, M.T.S., Asiri, A.M., 2016. Carbohydr. Poly. 148, 153–160; (f) Ali, N., Awais, Kamal, T., Ul-Islam, M., Khan, A., Shah, S.J., Zada, A., 2018. Int. J. Biol. Macromol. 111, 832–838.

Mahdavi, B., Paydarfard, S., Zangeneh, M.M., Goorani, S., Seydi, N., Zangeneh, A., 2019. Appl. Organometal. Chem. 33, e5248.

Manjunath, H.M., Joshi, C.G., 2019. Process Biochem. 82, 199–204.

McNamara, K., Tofail, S.A.M., 2013. Biomedical applications of nanoalloys. In: Florent, C. (Ed.), Nanoalloys: From Fundamentals to Emergent Applications. Elsevier, Oxford, p. 345.

McNamara, K., Tofail, S.A.M., 2015. Phys. Chem. Chem. Phys. 17, 27981.

McNamara, K., Tofail, S.A.M., 2016. Adv. Phys.: X 2 (1), 54–88.

Netala, V.R., Bethu, M.S., Pushpalatha, B., Baki, V.B., Aishwarya, S., Rao, J.V., Tartte, V., 2016. Int. J. Nanomed. 11, 5683–5696.

Park, S., Park, H.H., Kim, S.Y., Kim, S.J., Woo, K., Ko, G., 2014. Appl. Environ. Microbiol. 80, 2343.

Patil, M.P., Kim, G.-D., 2017. Appl. Microbiol. Biotechnol. 101, 79–92.

Patra, S., Mukherjee, S., Barui, A.K., Ganguly, A., Sreedhar, B., Patra, C.R., 2015. Mater. Sci. Eng. C 53, 298.

Sabale, S., Jadhav, V., Khot, V., Zhu, X., Xi, M., Chen, H., 2015. J. Mater. Sci. Mater. Med. 26, 1.

Sangami, S., Manu, M., 2017. Environ. Technol. Innov. 8, 150–163.

Shanmugasundaram, T., Radhakrishnan, M., Gopikrishnan, V., Pazhanimurugan, R., Balagurunathan, R., 2013. Colloids Surf. B Biointerfaces 111, 680–687.

Sriramulu, M., Sumathi, S., 2017. Adv. Nat. Sci. Nanosci. Nanotechnol. 8, 045012.

Stahl, M. et al, 2013. Ann. Oncol. 24, 51–56.

Surendra, M.K., Annapoorani, S., Ansar, E.B., Varma, P.H., Rao, M. R., 2014. J. Nanopar. Res. 16, 1.

Tansık, G., Yakar, A., Gündüz, U., 2014. J. Nanopart. Res. 16, 1.

Thun, M.J., Hannan, L.M., Adams-Campbell, L.L., 2018. PLoS Med. 5, e185.

World Cancer Research Fund, American Institute for Cancer Research, 2007. *Food, Nutrition, Physical Activity, and the Prevention of Cancer: A Global Perspective*. American Institute for Cancer Research, Washington, DC.

Zou, Y., Liu, P., Liu, C.H., Zhi, X.T., 2015. Biomed. Pharmacother. 69, 355.